# Model for photon migration in turbid biological media

**R. F. Bonner**

*Biomedical Engineering and Instrumentation Branch, National Institutes of Health, Bethesda, Maryland 20952*

**R. Nossal, S. Havlin, and G. H. Weiss**

*Physical Sciences Laboratory, Division of Computer Research and Technology, National Institutes of Health, Bethesda, Maryland 20952*

Received December 3, 1985; accepted October 31, 1986

Various characteristics of photon diffusion in turbid biological media are examined. Applications include the interpretation of data acquired with laser Doppler blood-flow monitors and the design of protocols for therapeutic excitation of tissue chromophores. Incident radiation is assumed to be applied at an interface between a turbid tissue and a transparent medium, and the reemission of photons from that interface is analyzed. Making use of a discrete lattice model, we derive an expression for the joint probability $\Gamma(n, \rho)d^2\rho$ that a photon will be emitted in the infinitesimal area $d^2\rho$ centered at surface point $\rho = (x, y)$, having made $n$ collisions with the tissue. Mathematical expressions are obtained for the intensity distribution of diffuse surface emission, the probability of photon absorption in the interior as a function of depth, and the mean path length of detected photons as a function of the distance between the site of the incident radiation and the location of the detector. We show that the depth dependence of the distribution of photon absorption events can be inferred from measured parameters of the surface emission profile. Results of relevant computer simulations are presented, and illustrative experimental data are shown to be in accord with the theory.

## 1. INTRODUCTION

In most *in vivo* clinical and research uses of light (other than those involving transparent tissues such as are found in the eye), incident radiation is applied to the interface between a turbid tissue and a transparent medium (air or water). Light that is reemitted at this interface into the external transparent medium can be analyzed to obtain information about parameters of photon interaction within the tissue.[1–4] Because photon mean free paths in tissue are typically of the order of 100 $\mu$m, photon diffusion models are often appropriate for interpreting optical measurements involving total path lengths of the order of 1 mm or more.[1,3,5,6] A good understanding of photon migration in turbid media can thus be quite useful when applying light, either therapeutically or diagnostically, to dense biological matter.

For example, laser Doppler blood-flow monitors are used in a number of diagnostic procedures.[7–10] In this case laser light is introduced at one point on a surface and collected at another point located approximately 0.5 to 1 mm away.[11] The emitted photons are analyzed for the mean magnitude of the Doppler shift, which is proportional to the root-mean-square (rms) blood cell speed.[12,13] Additionally, the fraction of the light that is Doppler shifted provides a measure of the number density of blood cells in the tissue. The calibration of these measurements depends on determining the path lengths, within the tissue, of the detected photons. Also, knowledge of the paths that detected photons move along while they are within the tissue is critical to understanding which tissue volumes are sampled and which parts of the microvasculature contribute to the flow signal.

Other techniques utilize light of several specific wavelengths, introduced at one point and detected at another on the surface of tissues, to determine the oxygenation of microvascular hemoglobin.[14–16] In this case the relative absorption of the different probing radiations is analyzed. The wavelength dependence of photon path lengths critically affects the calibration and accuracy of these and similar absorption techniques. In related schemes, the fluorescence of biological molecules such as nicotinamide-adenine dinucleotide, reduced[17,18] is used to quantify tissue metabolism or photochemistry. Knowledge of the distribution of photon paths is important in absolute quantitation of the measurements and in identifying which cells contribute to the signals.

Light is also used therapeutically to excite a variety of intrinsic and extrinsic chromophores, resulting either in thermal damage and tissue ablation or in photochemical excitation of cellular components (e.g., singlet oxygen production).[19,20] In these cases one is primarily concerned with the depth distribution of the site of photon absorption within a tissue and in being able to assess variations in this distribution as the wavelength is changed. Here, too, the only practical means of analyzing the interaction of light with the living tissue is to monitor the light that is diffusely reflected from the surface.

Thus there are several uses of light in tissue that are of considerable clinical importance for which additional understanding of photon interactions in turbid media might be beneficial. In this paper, therefore, we develop a theoretical model of photon migration in tissue. The present study is similar in spirit to that of Groenhuis *et al.*,[3,4] who show by a somewhat different analysis that surface emission can be used to infer scattering and absorption cross sections of bulk biological tissue. However, the emphasis here differs from that in previous publications in that by using a random-walk

0740-3232/87/030423-10$02.00 

model we are able to determine photon path lengths and path-depth distributions. Once the bulk scattering and absorption properties of a tissue are specified, our analysis can be used to deduce characteristics of the migration paths of those photons that contribute to diffuse surface reflectance measurements at any particular point. Similarly, the distribution of chromophore activation within a tissue can be determined.

For typical applications the radius of curvature and thickness of the tissue are greater than 1 cm. These values are very much greater than the length scale of scattering within the tissue, and a model of photon diffusion in which particles are injected perpendicularly to an infinite half-plane of turbid material is therefore applicable. "Trapping" of photons is deemed to occur either by emission of light from the planar surface (diffuse reflection) or by absorption into the bulk. Although we are interested primarily in optical applications, our analysis might pertain also to situations in which surface emission of neutrons is used to probe the interior properties of materials (e.g., petroleum exploration). The use of light to investigate turbulence within clouds might be described by a similar theory[21] because, in this case too, characteristic photon path lengths may be large compared with distances between scattering centers.

In Section 2 we analyze mathematically a three-dimensional lattice model that allows us to demonstrate relationships between photon diffusion within the tissue and easily measured surface intensity distributions. The main result of this paper is an expression for the probability distribution $\Gamma(n, \rho)\mathrm{d}^2\rho$ for the number of steps taken by a photon that is injected into the medium and subsequently emitted within a small area $\mathrm{d}^2\rho$ centered at $\rho = (x, y)$ relative to the point of injection. From this expression we are able to deduce expressions for the intensity distribution and total diffuse reflectance at the surface, the mean path length of detected photons as a function of the separation between emitting and detecting probes, and the probability of photon absorption as a function of depth.

The expressions that we derive have relatively simple forms. Although the present theory is but a first attempt to analyze some very complicated systems, the results should pertain to a variety of biomedically important measurements, particularly when the receiving and transmitting fibers of the probe are not too close to each other. Because of the complex structure of biological tissue it is impossible to specify precisely the physical details of photon migration, and the utility of our model will have to be established empirically. Although this work is similar in spirit to a number of diffusion theory calculations,[1-6] the aspect of lattice migration adopted here enables us to infer path-length distributions that are not readily obtainable either from conventional diffusion theory or from calculations based on transport theory.[3,22-30] Moreover, transport theory generally entails a great deal of numerical computation, which limits its utility in the simple applications that we envision.

Section 3 contains results of computer simulations that substantiate and extend our theoretical results. In Section 4 we illustrate how the present theory can be used to analyze real data obtained from living tissue. We also discuss several possibilities for further development of the model.

## 2. MATHEMATICAL ANALYSIS

Each of the applications that we have described involves a configuration in which light is incident primarily in the direction normal to the surface of a tissue mass that can be considered to be infinite in extent. (The probability that a photon reaches a tissue boundary other than the illuminated surface before being absorbed or reemitted is negligibly small.) Although biological tissues are complex structures, for many applications it suffices to consider models of homogeneous media that have the same average scattering and absorptive properties as do the corresponding real substances.

The model to be examined in the present paper is based on representing photon movement by a random walk in discrete time on a lattice. Since the approximations to be used imply that the number of steps is large, the model has certain features of a diffusion model. However, a lattice structure is necessary because the path length of a particle that performs continuous Brownian motion is known to be infinite. In order to establish a correspondence between a realistic picture of photon motion and the lattice model, we choose the lattice spacing $L$ to be the rms distance $\sigma$ traveled between successive scattering events. In terms of diffusion on a lattice, where the mean time interval between scattering events is $T$, the mean-square displacement of a photon in an infinite medium is thus given as

$$\langle r^2(t)\rangle \sim \sigma^2 t/T, \qquad t \gg T, \tag{1}$$

where $t$ is the elapsed time. We note that $t/T$ is the asymptotic average number of steps taken in time $t$.

We will assume that Beer's law applies to photon absorption within the medium. Thus, if the probability of survival (in an infinite medium) of a photon that travels for a distance $L$ is $\exp(-\nu L)$, we assign the absorption probability

$$\exp(-\mu) = \langle \exp(-\nu L)\rangle \tag{2}$$

per unit step for the lattice model. In this equation the right-hand side represents an average over all path lengths between successive collisions. Finally, our model consists of a random walk that takes place on a simple cubic lattice, the random walker being allowed to step to nearest neighbors only. Moreover, scattering is assumed to be isotropic (i.e., all scattering directions are equally probable, regardless of the incident direction). While this might appear to restrict the generality of the model, it can be shown that in the limit of a large number of anisotropic scattering events one can readjust parameters and the results can be fitted to those of the present analysis. Protons are considered to be injected (without reflection) at a single point on the surface $z = 0$ and detected (collected) at some other surface point. The entire surface $z = 0$ is a homogeneous absorbing barrier, and photons emitted from the surface are assumed not to return to the scattering medium. Our coordinate system is such that $z > 0$ corresponds to the interior. The first scattering event occurs within the first layer of scattering centers.

Most interesting properties of this random walk can be calculated in terms of the state probabilities $[Q_n(\mathbf{r})]$, where $Q_n(\mathbf{r})$ is the probability that the photon is at $\mathbf{r} = (x, y, z)$ at step $n$. The variables $(x, y, z)$ will be integers, it being

understood that a given lattice point corresponds to $(xL, yL, zL)$ in terms of the distance $L$. Since the surface $z = 0$ is absorbing, $Q_n(\mathbf{r})$ is subject to the boundary condition

$$Q_n(x, y, 0) = 0. \tag{3}$$

Furthermore, $Q_n(\mathbf{r})$ is to be found subject to the initial condition

$$Q_1(\mathbf{r}) = e^{-\mu}\delta_{x,0}\delta_{y,0}\delta_{z,1}, \tag{4}$$

where $\delta_{i,j}$ is a Kronecker delta. Equation (4) signifies that photons are injected into the medium along the $z$ axis and experience their first collision at the lattice point $(x = 0, y = 0, z = 1)$ (having been subjected to absorption while traveling to that point).

The $Q_n(\mathbf{r})$, which allow for absorption, can be expressed in terms of the Green's functions for random walks taking place on a fully infinite lattice in the absence of absorption. We designate the latter as $P_n(x, y, z|0, 0, 0)$ [to be abbreviated $P_n(x, y, z)$], which is the probability that a random walker that is initially at $(0, 0, 0)$ is at $(x, y, z)$ at step $n$. The $Q_n(\mathbf{r})$ can be written as

$$Q_n(\mathbf{r}) = [P_{n-1}(x, y, z - 1) - P_{n-1}(x, y, z + 1)]e^{-\mu n}, \tag{5}$$

the bracketed terms accounting for the boundary condition in Eq. (3), since by symmetry it follows that $P_n(\pm x, \pm y, \pm z) = P_n(x, y, z)$ (equivalent to the assumption of an unbiased random walk). The exponential factor is the probability of survival for $n$ steps. We therefore have reduced the problem of calculating the $Q_n(\mathbf{r})$ to the simpler one of finding $P_n(\mathbf{r})$. The latter, however, are known for lattice random walks: if we let

$$\lambda(\theta) \equiv \tfrac{1}{3}(\cos\theta_1 + \cos\theta_2 + \cos\theta_3) \tag{6}$$

be the structure factor[31] of a nearest-neighbor random walk on a simple cubic lattice, then $P_n(\mathbf{r})$ is given as

$$P_n(\mathbf{r}) = \frac{1}{(2\pi)^3}\int\int_{-\pi}^{\pi}\int \lambda^n(\theta)\exp[-i(x\theta_1 + y\theta_2 + z\theta_3)]\mathrm{d}^3\theta. \tag{7}$$

We will be interested in large $n$, in which limit a standard argument in random-walk theory[31] or central-limit theory allows us to approximate $P_n(\mathbf{r})$ by

$$P_n(\mathbf{r}) \approx \left(\frac{3}{2\pi n}\right)^{3/2}\exp\left[-\frac{3}{2n}(x^2 + y^2 + z^2)\right]. \tag{8}$$

Having calculated $P_n(\mathbf{r})$, we can turn our attention to the calculation of properties of radiation absorbed at the surface, which constitute the observable information. The joint probability that a photon will be absorbed at step $n$ at the point $\rho = (x, y)$ on the surface is

$$\Gamma(n, \rho) = \tfrac{1}{6}Q_{n-1}(x, y, 1)\exp(-\mu), \tag{9}$$

since absorption can occur only following a configuration in which the random walker is one lattice point removed from the absorbing surface. On substituting expression (8) into Eq. (5) and then into Eq. (9), we find that $\Gamma(n, \rho)$ is given as

$$\Gamma(n, \rho) = \frac{\sqrt{3}}{2}\left(\frac{1}{2\pi(n-2)}\right)^{3/2}(1 - e^{-6/(n-2)}) \times \exp\left(\frac{-3\rho^2}{2(n-2)} - \mu n\right), \tag{10}$$

where $\rho^2 = \rho\cdot\rho = x^2 + y^2$. When $n$ is large, which is the limit that we are working in, only $\rho \gg 1$ will be of interest, so that we can regard $\Gamma(n, \rho)$ as having circular symmetry. The total amount of energy emitted in a circle of radius between $\rho$ and $\rho + \mathrm{d}\rho$ is

$$\gamma(\rho)\mathrm{d}\rho = 2\pi\rho\Gamma(\rho)\mathrm{d}\rho \equiv 2\pi\rho\sum_{n=2}^{\infty}\Gamma(n, \rho)\mathrm{d}\rho \simeq 2\pi\rho\mathrm{d}\rho\int_0^{\infty}\Gamma(n + 2, \rho)\mathrm{d}n. \tag{11}$$

In this approximation one has, from Eq. (10),

$$\Gamma(\rho) = (2\pi\rho)^{-1}\gamma(\rho) = \frac{1}{4\pi\rho}\left\{\exp(-\rho\sqrt{6\mu}) - \frac{\rho}{\sqrt{\rho^2 + 4}}\exp[-\sqrt{6\mu(\rho^2 + 4)}]\right\}e^{-2\mu}, \tag{12}$$

which implies that the total amount of radiation diffusely reflected from the surface is

$$\int_0^{\infty}\gamma(\rho)\mathrm{d}\rho = \frac{1}{\sqrt{24\mu}}[1 - \exp(-\sqrt{24\mu})]e^{-2\mu}. \tag{13}$$

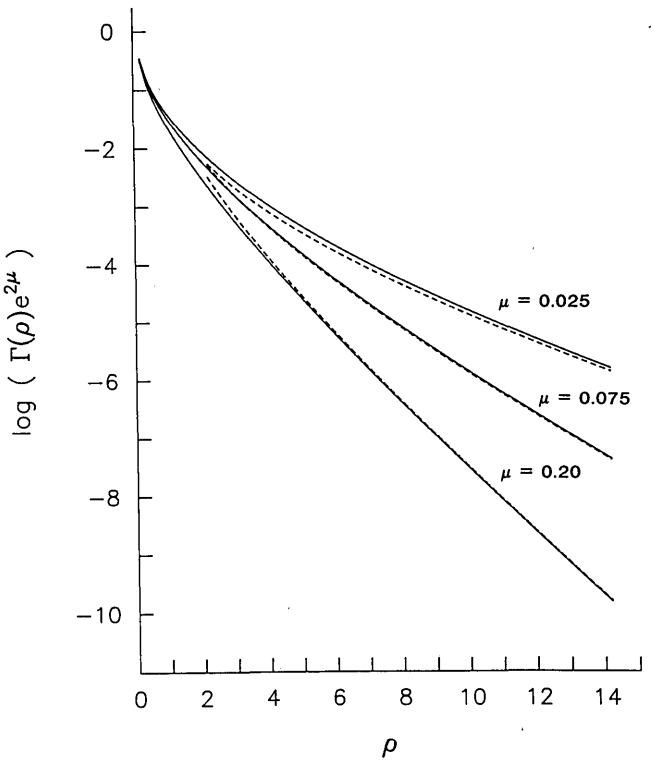


Fig. 1. The logarithm of the surface emission intensity $\Gamma(\rho)e^{2\mu}$ for various values of absorption coefficient, calculated according to Eq. (12). The dashed lines are corresponding curves calculated according to the approximation given in expression (14).

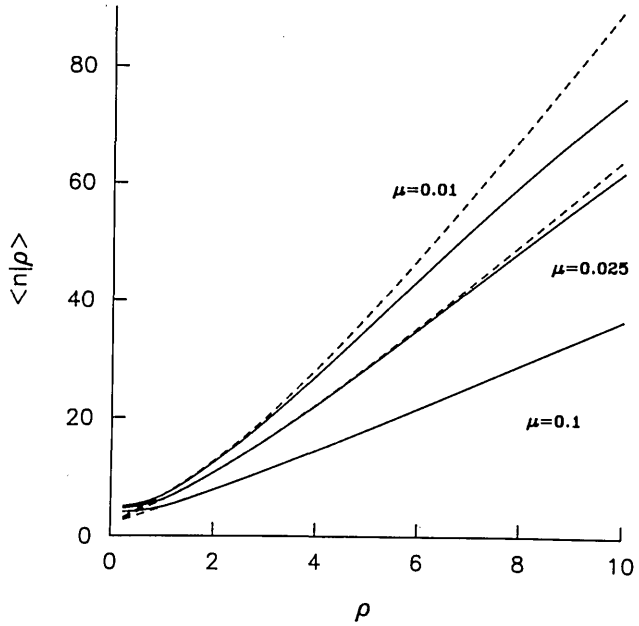


Fig. 2. Expected number of steps taken by a photon before it is reemitted at the surface, given as a function of the distance along the surface between the point of insertion and the point of emission. The solid line has been calculated by using Eq. (15), and the dashed line has been obtained from the approximate form given in expression (16). The agreement is particularly good for higher values of the absorption coefficient $\mu$.

The expression for $\Gamma(\rho)$, given by Eq. (12), is the point intensity of the reemitted radiation. For sufficiently large values of $\rho$, Eq. (12) can be rewritten as (see Fig. 1)

$$\Gamma(\rho) \approx \frac{\sqrt{6\mu}}{4\pi\rho^2} e^{-2\mu} \exp(-\rho\sqrt{6\mu}). \tag{14}$$

A quantity that is of direct interest (see, e.g., Fig. 9 below) is the expected number of steps taken by a photon before it is reemitted at the surface $z = 0$. This is defined by the relation

$$\langle n|\rho\rangle \equiv \sum_{n=2}^{\infty} n\Gamma(n,\rho) \Big/ \sum_{n=2}^{\infty} \Gamma(n,\rho) \tag{15}$$

$$\approx \frac{\int_0^{\infty} (n+2)\Gamma(n+2,\rho)\mathrm{d}n}{\int_0^{\infty} \Gamma(n+2,\rho)\mathrm{d}n} = 2 + \rho\sqrt{\frac{3}{2\mu}}$$

$$\times \left( \frac{1 - \exp\{\sqrt{6\mu}[\rho - (\rho^2+4)^{1/2}]\}}{1 - \dfrac{\rho}{(\rho^2+4)^{1/2}} \exp\{\sqrt{6\mu}[\rho - (\rho^2+4)^{1/2}]\}} \right). \tag{16}$$

The latter expression is a useful approximation when $\mu > 0.025$. A comparison of the expressions for $\langle n|\rho\rangle$, as given by Eq. (15) and expression (16), is shown in Fig. 2. As can be seen from the figure, the agreement between the two forms is excellent at $\mu = 0.1$ and shows significant deviations for $\mu = 0.01$. The expression in Eq. (16) indicates that $\langle n|\rho\rangle$ is approximately proportional to $\rho$, being given as

$$\langle n|\rho\rangle \approx 2 + 3\rho/\sqrt{6\mu}, \qquad \rho^2 \gg 4. \tag{17}$$

Figure 3 shows the behavior of the coefficient of variation

$$C = \sigma(n|\rho)/\langle n|\rho\rangle, \tag{18}$$

where $\sigma(n|\rho) \equiv (\langle n^2|\rho\rangle - \langle n|\rho\rangle^2)^{1/2}$. The significant feature of the curves is that they decrease as a function of $\rho$. This indicates that photons that travel long distances before escaping from the surface tend to have trajectories whose projections onto the surface lie close to $\rho$. In addition, they remain close to the surface, as otherwise their chance of being trapped in the interior is greatly increased. We will see a confirmation of this later when we calculate some statistical properties of the maximum depth reached by photons that ultimately migrate to the surface (see Fig. 10 below).

So far we have discussed statistical properties of photons that escape from the lattice. We next consider some corresponding properties of photons that are trapped in the interior. The probability that a photon is absorbed at $\mathbf{r} = (x, y, z), z > 0$, after having completed the $(n-1)$st step but before subsequent scattering, is

$$g_n(\mathbf{r}) = Q_n(\mathbf{r}) \cdot (1 - e^{-\mu})$$

$$= (1 - e^{-\mu})[P_{n-1}(x,y,z-1) - P_{n-1}(x,y,z+1)]e^{-\mu n}. \tag{19}$$

Therefore, by using the integral approximation introduced earlier, we can write for the probability of absorption at $z$

$$g(z) \sim \int_1^{\infty} \mathrm{d}n \int_{-\infty}^{\infty}\int \mathrm{d}x\mathrm{d}y g_n(r) \sim \exp(-z\sqrt{6\mu}), \tag{20}$$

which decreases exponentially with $z$. The average depth at which absorption occurs is therefore

$$\langle z\rangle_a \equiv \sum_{z=1}^{\infty} zg(z) \Big/ \sum_{z=1}^{\infty} g(z) = 1/[1 - \exp(-\sqrt{6\mu})], \tag{21}$$

which increases slowly as $\mu$ decreases. Thus, for $\mu = 0.1$ we find that $\langle z\rangle_a = 1.8$, while for $\mu = 0.025$ we have $\langle z\rangle_a = 3.1$.

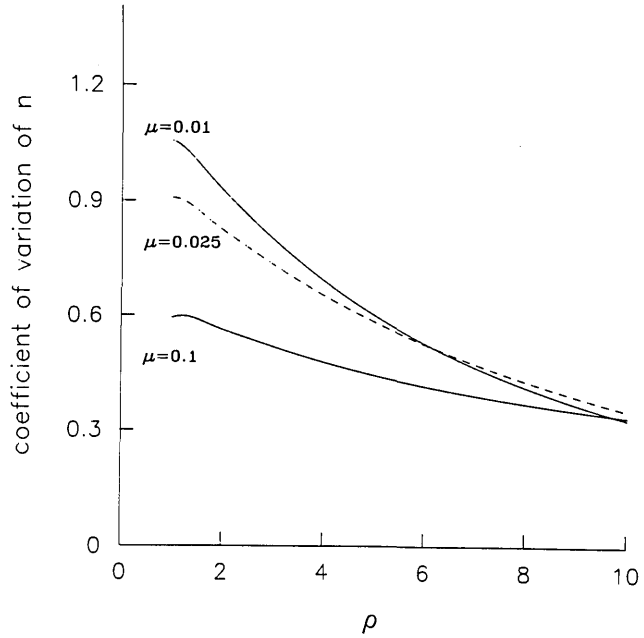


Fig. 3. Coefficient of variation $C(\rho) \equiv (\langle n^2|\rho\rangle - \langle n|\rho\rangle^2)^{1/2}/\langle n|\rho\rangle$ of photons emerging at a distance $\rho$ from the point of insertion, calculated by using Eqs. (10) and (15) and a similar equation for $\langle n^2|\rho\rangle$.

The average number of steps until an interior absorption occurs also can be found in terms of $g_n(\mathbf{r})$ and is given in the integral approximation as

$$\langle n\rangle_a \approx \sum_{n=1}^{\infty}\sum_{z=1}^{\infty} n\int_{-\infty}^{\infty}\int g_n(\mathbf{r})\mathrm{d}x\mathrm{d}y \Big/ \sum_{n=1}^{\infty}\sum_{z=1}^{\infty}\int_{-\infty}^{\infty}\int g_n(\mathbf{r})\mathrm{d}x\mathrm{d}y$$

$$\approx 1 + \int_0^{\infty} n^{1/2}(1+e^{-3/(2n)})e^{-\mu n}\mathrm{d}n \Big/ \int_0^{\infty} n^{-1/2} \times (1+e^{-3/(2n)})e^{-\mu n}\mathrm{d}n$$

$$= 1 + \frac{1}{2\mu}\left[\frac{1+(1+\sqrt{6\mu})\exp(-\sqrt{6\mu})}{1+\exp(-\sqrt{6\mu})}\right]. \tag{22}$$

As one expects, this function decreases when the absorption parameter $\mu$ increases.

It also is of interest to find a parameter characterizing the depth to which a typical photon will penetrate. One of the simplest of such parameters is the maximum depth $z = Z$ that the photon reaches before it is ultimately absorbed. In order to calculate the statistical properties of this random variable we need to replace the expression in Eq. (5) for $Q_n(\mathbf{r})$ with one that takes account of a second absorbing barrier at $z = Z$. The purpose of this second barrier is to permit the enumeration of the properties of random walks that penetrate to a depth of exactly $Z$. If $\Gamma(\rho|Z)$ denotes the probability that a random walk is absorbed at a point $(x, y, 0)$ on the surface, given that it has not been absorbed at the second barrier at $z = Z$, then the probability that it is absorbed at $\rho$, having visited $z = Z$ at least once, is $\Gamma(\rho|Z+1) - \Gamma(\rho|Z)$. Hence we must find an expression for $\Gamma(\rho|Z)$. Let $Q_n(\rho, z|Z)$ be the probability of being at $\rho$ at step $n$ of the random walk when there is an absorbing barrier at $z = Z$. $\Gamma(\rho|Z)$ can then be expressed as

$$\Gamma(\rho|Z) = e^{-\mu}\sum_{n=1}^{\infty} Q_n(\rho, 1|Z)/6, \tag{23}$$

so that as a start we must find an expression for $Q_n(\rho, 1|Z)$. Since $z = Z$ is a perfectly absorbing boundary, one can use the method of images or a Poisson transformation to show that $Q_n$ is given as

$$Q_n(\rho, 1|Z) = \sum_{l=-\infty}^{\infty}\{P_{n-1}(\rho, 2lZ) - P_{n-1}(\rho, 2+2lZ)\}e^{-\mu n}. \tag{24}$$

After summing this expression over $n$ and using the Gaussian approximation for $P_n(\mathbf{r})$, one obtains

$$4\pi\Gamma(\rho|Z) \approx \sum_{l=-\infty}^{\infty}\left(\frac{\exp[-\sqrt{6\mu(\rho^2+4l^2Z^2)}]}{\sqrt{\rho^2+4l^2Z^2}} - \frac{\exp\{-\sqrt{6\mu[\rho^2+4(1+lZ)^2]}\}}{\sqrt{\rho^2+4(1+lZ)^2}}\right)e^{-2\mu}, \tag{25}$$

which is the probability of being absorbed at $\rho$, not having penetrated to a depth $Z$. In the presence of an absorbing barrier at $z = Z$ the total amount of radiation emitted at $z = 0$ is approximately

$$R_0(Z) \approx 2\pi\int_0^{\infty}\rho\Gamma(\rho|Z)\mathrm{d}\rho$$

$$= \frac{1}{\sqrt{24\mu}}\left[1 + 2\sum_{l=1}^{\infty}\exp(-lZ\sqrt{24\mu}) - \sum_{l=-\infty}^{\infty}\exp(-|1+lZ|\sqrt{24\mu})\right]e^{-2\mu}$$

$$= \frac{1}{\sqrt{24\mu}}\left\{1 - \exp(-\sqrt{24\mu}) + \frac{2[1-\cosh(\sqrt{24\mu})]}{\exp(Z\sqrt{24\mu})-1}\right\}e^{-2\mu}. \tag{26}$$

When $Z = \infty$, this reduces to the result obtained earlier in Eq. (13), and when $Z = 1$, $R_0(Z)$ reduces to 0, as it should. It is evident from this expression (26) that for all but the thinnest of layers, the absorbing boundary at $z = Z$ can be neglected. For example, when $\mu = 0.025$, one finds that $R_0(\infty) = 0.696$, $R_0(5) = 0.552$, and $R_0(10) = 0.693$, so that with 10 layers the effect of the second boundary is negligible. If the absorption parameter $\mu$ is increased, a correspondingly smaller number of layers allows the same conclusion to be drawn.

Finally, the probability that a photon trapped on the surface at a distance $\rho$ from its entrance point will penetrate to a maximum depth $Z$ is

$$U(Z|\rho) = [\Gamma(\rho|Z+1) - \Gamma(\rho|Z)]/\Gamma(\rho). \tag{27}$$

This expression allows us to calculate both the distribution of the maximum depth and the moments of this variable. The expressions for the first and second moments can formally be given as

$$\langle Z\rangle = \sum_{j=1}^{\infty}[1 - \Gamma(\rho|j)/\Gamma(\rho)],$$

$$\langle Z^2\rangle = \sum_{j=1}^{\infty}(2j-1)[1 - \Gamma(\rho|j)/\Gamma(\rho)]. \tag{28}$$

By using these formulas, we have calculated $\langle Z\rangle$ and $\sigma(Z) \cong (\langle Z^2\rangle - \langle Z\rangle^2)^{1/2}$ as a function of $\rho$, finding that these parameters can be fitted quite well by the following empirically determined formulas

$$\langle Z\rangle = a + b\rho^{2/3}, \qquad \sigma(Z) = a' + b'\rho^{1/4}, \tag{29}$$

where $a$, $a'$, $b$, and $b'$ depend on $\mu$. Results of calculating $\langle Z\rangle$ and $\sigma(Z)$ as a function of $\rho$, both exactly and from the approximations given in Eq. (29), are compared in Fig. 4. It can be seen from Eq. (29) that the coefficient of variation $C = \sigma(Z)/\langle Z\rangle$ decreases monotonically to zero except at the lowest values of $\rho$.

## 3. SIMULATIONS

Computer simulations of photon diffusion were performed in order to test the mathematical analysis of the preceding section. In all instances the following characteristics were assumed: (1) photons can be represented by random walkers migrating within an "infinite" three-dimensional medi-

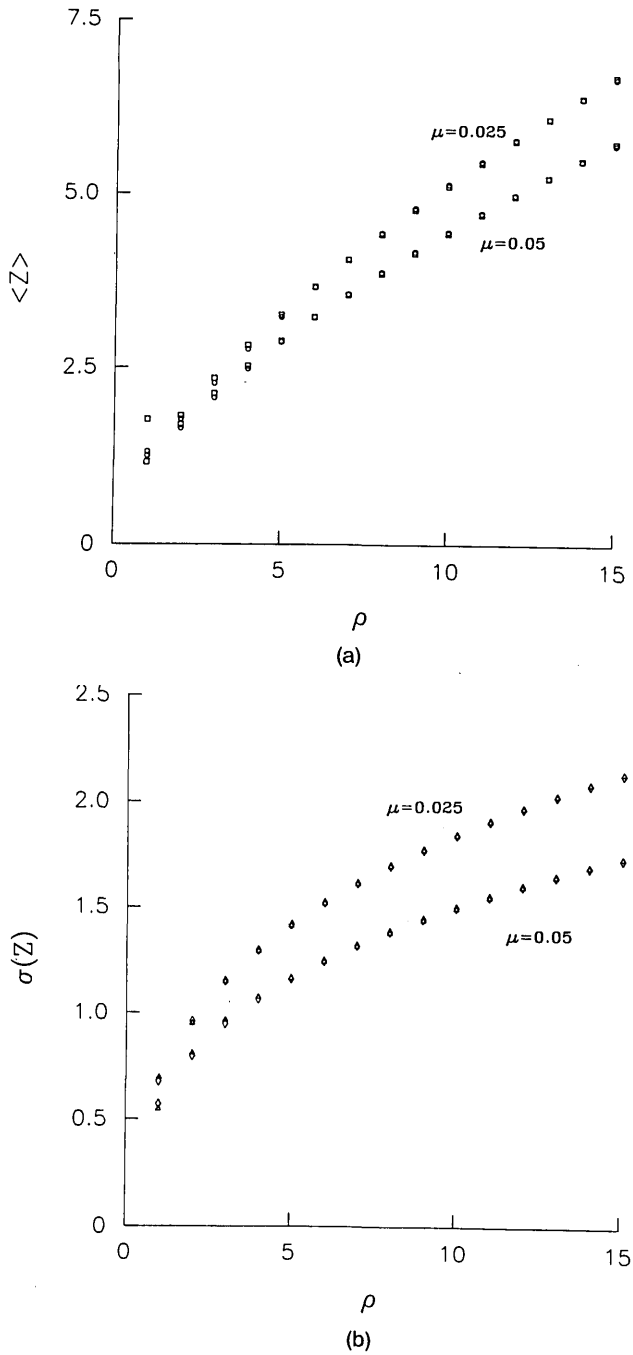


Fig. 4. (a) The expected value of maximum depth $\langle Z \rangle$; (b) the variance $\sigma(Z)$, given as a function of the exit distance $\rho$. No discernible difference is noted between results calculated from Eq. (28) and data points obtained by fitting according to the forms given in Eq. (29).

um bounded by a surface plane located at $z = 0$; (2) photons are injected without reflection into that medium at a single point on the plane $z = 0$, in a direction of normal incidence; (3) photons can be absorbed during each diffusion step with a probability of $e^{-\mu}$; (4) the scattering-angle distribution is isotropic, and successive photon steps are uncorrelated; and (5) when photons return to the surface $z = 0$ they are emitted without reflection and collected.

Monte Carlo simulations were performed for a cubic lattice in which all steps are unit vectors along the $x$, $y$, and $z$ axes. For comparison, we also investigated a continuum model in which the step lengths are exponentially distributed with a mean length $L_0$ (Beer's law) and in which all scattering angles are equally likely (i.e., scattering is not restricted to be along the lattice axes). The Monte Carlo simulations on the discrete lattice are used to assess the mathematical approximations needed to derive the analytic expressions given in Section 2. The simulations of the continuum model, which mimic Beer's law scattering, serve to test the validity of the basic physical approximations implicit in the discrete lattice formulation of the diffusion process. Note that, according to the discussion preceding Eq. (1), the lattice spacing $L$ is related to the mean length $L_0$ of an exponential distribution as $L = \sqrt{2}\,L_0$. The absorption coefficient for the continuum Monte Carlo calculations also must be assigned; in the continuum simulations reported in this paper, the number of surviving photons after each randomly generated step of length $l_i$ was taken to be $\exp(-\tilde{\mu} l_i)$, and correspondence with the absorption coefficient $\mu$ for the discrete lattice model is achieved by setting $\tilde{\mu} = \mu/\sqrt{2}$.

Equation (12) and expression (14) provide expressions for $\Gamma(\rho)$, the probability density of emitted photons (normalized per unit area), given as a function of the distance from the point of injection to the point of emission from the surface. The distance along the surface, $\rho$, is given in units of the rms scattering length when Eq. (12) is used to calculate the emission profile. Thus, in order to compare these theoretical expressions with emission profiles computed by a continuum Monte Carlo model having a run-length distribution given as $\exp(-l_i)$, the distance axis of the latter has to be contracted by the factor $(2)^{1/2}$. Also, if the absorption parameter in Eq. (12) is $\mu$, the absorption coefficient for the corresponding continuum Monte Carlo calculation is $\mu/(2)^{1/2}$.

As shown in Figs. 5 and 6, the Monte Carlo simulations confirm the appropriateness of the analytical expressions (cf. Fig. 1). They explicitly demonstrate a strong dependence of $\Gamma(\rho)$ on the absorption coefficient $\mu$ as well as an implicit dependence on the lattice spacing $L$. The spatial

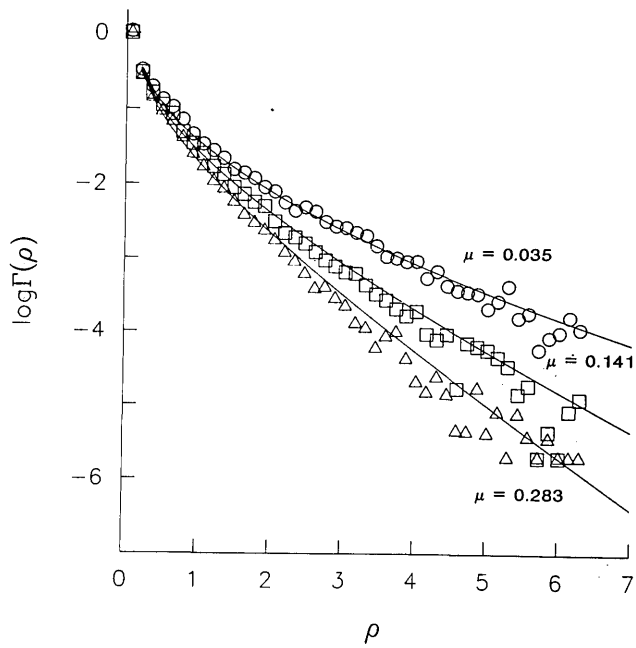


Fig. 5. Emission intensity as a function of $\rho$. Comparison between analytical results given by Eq. (12) (solid lines) and results of Monte Carlo calculations for the continuum model.

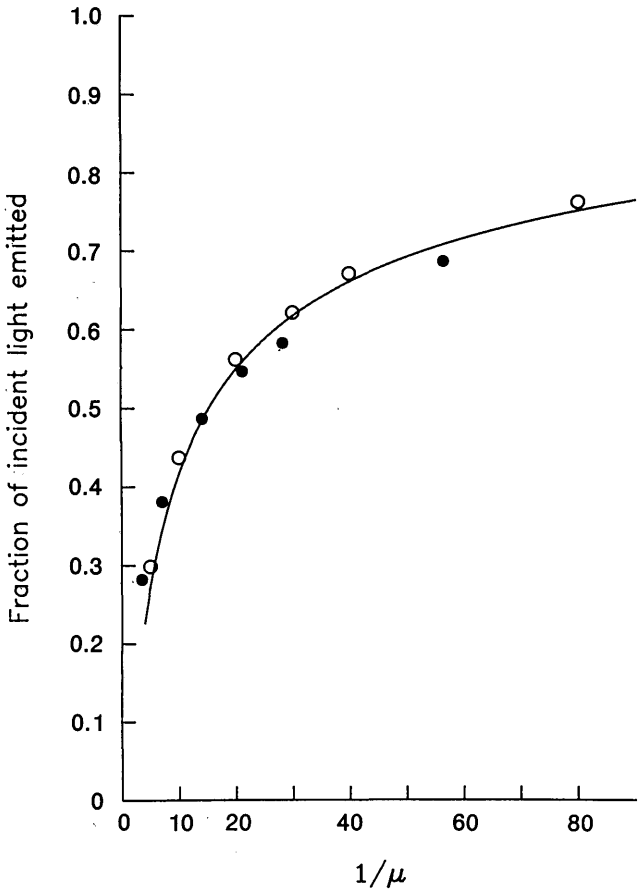


Fig. 6. Total reflectance, given in terms of the inverse absorption coefficient $1/\mu$. Values shown as a solid line were calculated from Eq. (13). The open circles are the results of Monte Carlo calculations for a cubic lattice, and the filled circles are the results of Monte Carlo calculations for the isotropic continuum model.

distribution of diffusely reflected photons is readily measured noninvasively and should be particularly useful in empirical evaluations of living biological tissue. This result implies that both an effective mean free path for isotropic scattering, $L_0$, and the absorption coefficient, $\mu$, can be ascertained from the surface intensity profile if one or the other of the parameters can be independently determined. However, because the shape of $\Gamma(\rho)$ at large values of $\rho$ is very sensitive to changes in $\mu$, even if independent measurement is not feasible, a good estimate of $\mu$ and $L_0$ can be obtained. Although the surface profile expressions given in Eq. (12) and expression (14) were derived for an isotropic scattering model, we have found similar results when anisotropic angular scattering is taken into account. (Additional studies are currently under way to investigate further the applicability of this model and its limitations.)

The surface emission profiles described by Eq. (12) are indeed experimentally observed. In Fig. 7 we show, as an illustration, the results of measurements on human forearm skin made with a laser Doppler blood-flow monitor (Laserflo, TMI Inc., Minneapolis, Minn.). The instrument had been outfitted with a special probe that allowed variations in the distance $r$ between the incident beam and the detector. Incident and emitted radiation were transported along 65-$\mu$m-diameter fibers that could be separated by distances varying from 0.3 to 3.3 mm. [In one case (see Fig. 7) data were augmented by results obtained from a video system, which extended the distance to 4.5 mm.] When a laser diode ($\lambda$ = 780 nm) or a He–Ne laser ($\lambda$ = 633 nm) was used as a light source, the intensity profile exhibited a slowly decreasing "tail" at large $r$, which is predicted by our model. However, when the emission from an argon-ion laser ($\lambda$ = 516 nm) was used as the probe radiation, the intensity profile was much sharper. This, too, is expected from the theory, because in this case the tissue absorption coefficient is greater. The behavior of $\Gamma(r)$ at small values of $r$ is determined largely by the scale factor associated with the effective mean free path of isotropic scattering, $L$, whereas the behavior at larger $r$ is affected by the absorption coefficient $\mu$. This can be explained by the fact that for small values of $\rho = r/L$ the mean path lengths of photons that leave the tissue are short, whereas the probability that a photon will survive as it traverses the relatively long paths necessary to reach a detector located far from the point of incidence is strongly affected by absorption. An approximate estimate of $L$ can be obtained from the characteristics of $\Gamma(r)$ at smaller values of $r$.

An analytical expression for the mean path length $\langle n|\rho\rangle$ of photons emitted at distance $\rho$ from the point of injection is given by expression (16) and has the behavior illustrated in Fig. 2. The most significant characteristic is the linear dependence of $\langle n|\rho\rangle$ on $\rho$, for $\rho > 2$, with a proportionality coefficient that varies as $1/(6\mu)^{1/2}$ [cf. Eq. (17)]. Monte Carlo simulations verify this somewhat surprising behavior; in Fig. 8(a) we show the asymptotic values of the slope $\langle n|\rho\rangle/\rho$, as a function of $\mu$, determined both from Monte Carlo

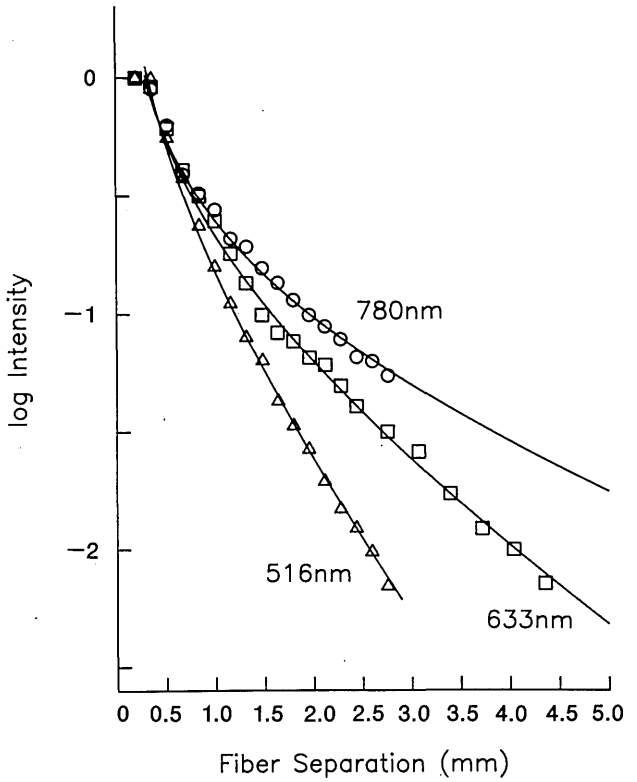


Fig. 7. Emission intensity measurements, as a function of the distance between the incident source and the detector, of light diffusing within human forearm skin, as determined with a laser Doppler blood-flow monitor. The solid lines are least-squares fits to the data ($R^2 > 0.99$), obtained by using Eq. (12). (Parameters are given in Table 1.) Note that the intensity decreases more rapidly, as a function of $\rho$, for shorter wavelength radiation (for which tissue absorption is greater).

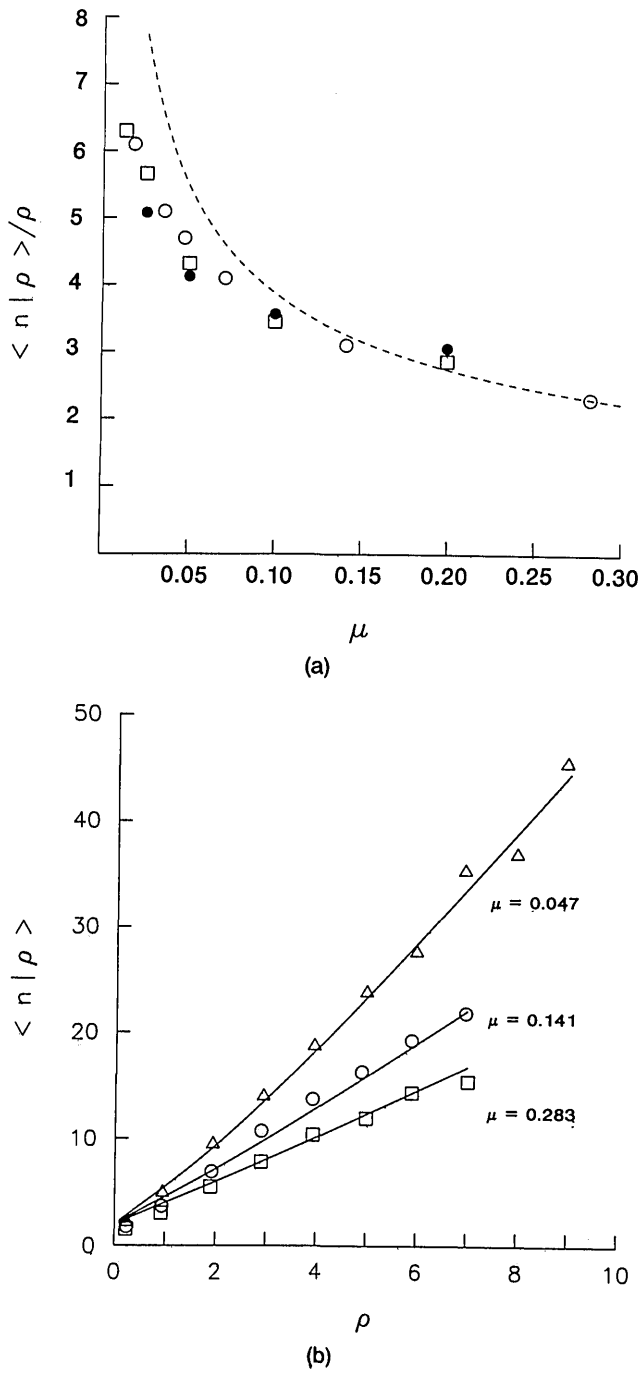


Fig. 8. (a) Values of the asymptotic slope, $\langle n|\rho\rangle/\rho$, determined from plots of the expected value of path lengths of photons emitted at surface distance $\rho$, ascertained for different values of $\mu$. Symbols: □, Monte Carlo (cubic lattice); ○, Monte Carlo (continuum model); ●, slope determined from expression (16) when calculated from values of $\rho \lesssim 10$. The dotted line is the limiting slope at very high $\rho$, as determined by Eq. (17). (b) Typical results of Monte Carlo calculations for the isotropic continuum model. Note that in this case $\langle n|\rho\rangle$ is linear with $\rho$, even for vanishingly small values of $\rho$. The lines are obtained from expression (16).

calculations and from expression (16). We also see in Fig. 8(b) that the linear dependence of $\langle n|\rho\rangle$ holds for the Beer's law continuum model, even as $\rho$ tends to 0 [see Fig. 8(b)]. The solid curves in Fig. 8(b) have been calculated from expression (16), and we conclude that the mathematical approximations implicit in expression (8) are particularly appropriate when the discrete lattice is replaced by a model that more closely represents tissue.

Knowledge of the mean photon path between two points separated by a (real) distance $r$ on the surface of tissues, $\langle n|r\rangle$, is often critical when quantifying noninvasive optical measurements (for example, in evaluating blood volume and flow parameters from Doppler-shifted signals[12] and in analyzing the absorption of light within a tissue mass[20,32]). According to our model, $\langle n|r\rangle$ can be determined from the parameters $L_0$ and $\mu$ obtained from the surface emission profiles. Experimental evidence is presented in Fig. 9 that shows the behavior between $\langle n\rangle$ and $r$ as predicted by expression (16). Measurements were made with the same laser Doppler blood-flow monitor used to obtain the data shown in Fig. 7 (again, for human forearm skin with a variable spacing probe, $\lambda = 633$ nm). This instrument allows us to determine the average number of times that a photon collides with a moving red cell before leaving the tissue (calculated from the fraction of the light that is Doppler shifted, which is designated as "blood volume" on the face of the instrument), the latter being proportional to the path length of photon migration. The data points denoted by circles pertain to resting skin, and those denoted by squares pertain to vasodilated tissue. The lines were calculated from expression (16), using values of $\mu$ and $L$ obtained from the data shown in Fig. 7 and scaled by appropriate factors along the ordinates. (These scale factors can be used to determine the mean distance that a photon diffuses before being Doppler shifted, from which one can ascertain the number density of red cells in the tissue.)

It also may be desirable to know how deeply photons might have penetrated within a tissue. The probability of a photon's being absorbed at depth $z$ is shown by expression (20) to decrease exponentially with distance from the sur-

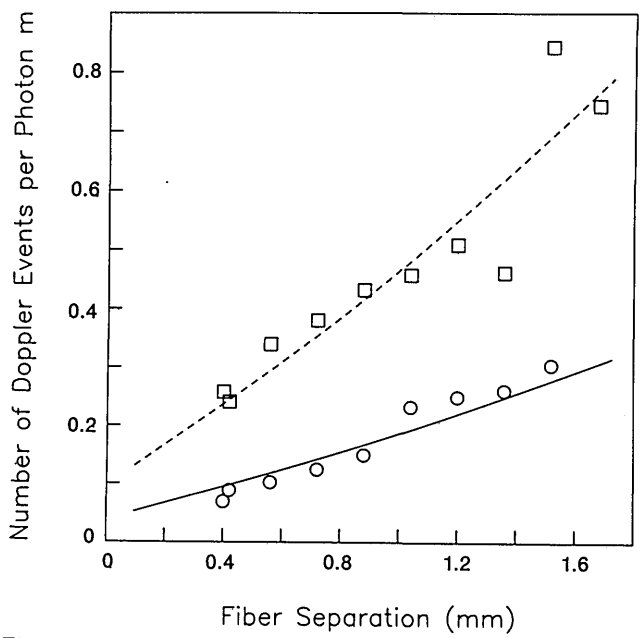


Fig. 9. Average number of times that a photon collides with moving red cells versus distance along the surface, measured in human forearm skin with a laser blood-flow monitor. Data were obtained with a probe that enabled the distance between points of photon injection and detection to be varied (○, resting skin; □, vasodilated skin).

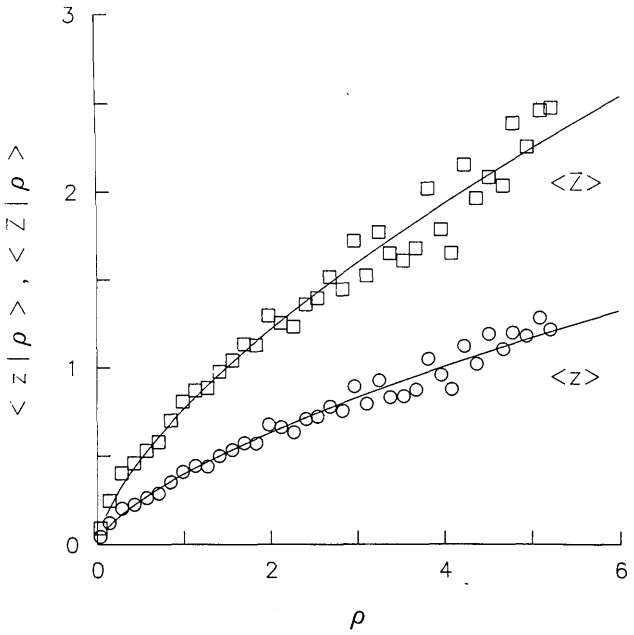


Fig. 10. Comparison between expected values of maximum $\langle Z \rangle$ and average $\langle z \rangle$ depths experienced by photons that emerge at distance $\rho$. Points are obtained from Monte Carlo simulations for isotropic continuum model. Curves are fitted according to the analytical form shown in Eq. (29). ($\mu = 0.047$.)

face, with an apparent absorption coefficient $(6\mu)^{1/2}$. Since we assume that the tissue has homogeneous absorption characteristics, this distribution is identical to the depth distribution of photon flux. Knowledge of the latter quantity is critically important in therapeutic uses of light if one wishes to determine dosimetry of different cell layers. Thus the relationship shown in expression (14) is of particular interest. The logarithms of the depth distribution $g(z)$ given by expression (20) and the quantity $\rho^2\Gamma(\rho)$ [cf. Eq. (12)] have the same slope, indicating that one can ascertain the depth distribution by measuring the intensity at the surface of the tissue. In other words, the depth distribution and a simple function of the surface intensity both vary as $\exp(-\alpha r)$, where $r$ is the actual distance and the decay constant is $\alpha = (\nu/L_0)^{1/2}$ [see Eq. (2)].

Finally, when light is used diagnostically, it frequently is important to know the depth distribution of the diffusive paths of photons emerging at a given point on the surface. This distribution corresponds to the average residency time at a given depth $z$. Figure 10 shows the first moment of the depth probability distribution, $\langle z \rangle$, as determined by Monte Carlo simulation for selected exit distances $\rho$, compared with the average value of the maximum depth, $\langle Z \rangle$. We note that both quantities have the functional dependence given in Eqs. (29) and that the expected value of the maximal depth is approximately twice the mean depth.

## 4. DISCUSSION

Several optical procedures for diagnosis and therapy currently are being applied to diverse tissues, the internal structure of which may differ quite significantly. Skeletal muscle, for instance, contains highly organized protein networks that result in periodic variations in the index of refraction of the order of 1-$\mu$m length scale. It also contains large concentrations of the visible chromophore myoglobin. In contrast, brain and skin tissues have smaller and less-organized refractile elements and variable levels of visible chromophores (e.g., melanin). The use of light on such different tissues for either diagnostic measurements or phototherapy may yield dramatically different results, in part because of differences in scattering and absorption properties and hence differences in photon paths in the tissues. Large changes in the absorption and scattering coefficients with changes in photon wavelength can also have dramatic effects in any given tissue.

The photon diffusion theory developed in this study relates the scattering and absorption parameters $L$ and $\mu$ to easily measured surface profiles of photons diffusely emitted from a planar interface between a transparent medium and a turbid tissue. These surface profiles can be measured on living tissues (the optical properties of which may change dramatically with excision and fixation). Once the characteristic scattering and absorption parameters for a given living tissue are obtained for the wavelength(s) to be used in diagnosis or therapy, other relevant information can be obtained according to the model. For instance, one can infer the mean photon path length, the depth distribution of photon flux, and the average depth of the cell layers being analyzed by a particular clinical technique.

Biological tissues contain a high density of refractile elements whose size is of the order of the wavelength of light. Therefore individual scattering events are very frequent and highly anisotropic (the scattering angle distribution for a single scattering event is usually strongly skewed in the forward direction). Thus the path length for isotropic scattering $L$ in this theory really represents an optical parameter related to the sum of several low-angle scattering steps that randomize the incident photon direction. We are currently investigating how optical anisotropy might affect the present analysis. Preliminary results, based on both Monte Carlo simulations and stochastic theory, indicate that the surface emission intensity $\Gamma(\rho)$ is indeed a universal function when expressed in terms of an appropriately scaled length variable.

In view of the mathematical approximations used to obtain Eq. (10), we expected the current theory to be correct only for values of $\rho$ greater than two or three times the value of an appropriately defined step length. Yet the data shown in Figs. 7 and 9 suggest that the theory holds to even smaller values of $\rho$ ($r \lesssim 0.3$ mm; i.e., $\rho \lesssim 0.6$). Table 1 contains values of the diffusion parameters $L$ and $\mu$ of living forearm skin, determined from the surface intensity distributions shown in Fig. 7. As can be seen, the parameters for each of three wavelengths predict light transmission similar to published results that were obtained by *in vitro* studies on excised specimens.[32,33] Because our measurements were performed on intact live skin, exact comparisons are difficult to make. It should be noted, however, that an *in vivo* measurement scheme, such as ours, yields values more appropriate to clinical use.

For most tissues, the determination of an effective absorption parameter, $\mu$, probably does not depend significantly on the detailed characteristics of anisotropic scattering. However, the situation may be quite different for strongly pigmented structures such as those found in the retinas of some animals or in certain diseases (e.g., malignant melanoma).

**Table 1. Predictions, from *in Situ* Data, of Transmission through Skin, Compared with Literature Values Determined from *in Vitro* Measurements in Excised Tissue**

| λ (nm) | Fitted Parameters[a] | | 1/*e* Depth (mm) | | |
|---|---|---|---|---|---|
| | $\mu$ | $L^{-1}$ (mm$^{-1}$) | Predicted[b] | Measured[c] | Applied[d] |
| 785 | 0.048 | 0.48 | 1.35 | 0.89 | 1.15 |
| 633 | 0.138 | 0.51 | 0.98 | 0.54 | 0.61 |
| 516 | 0.697 | 0.50 | 0.66 | – | 0.26 |

[a] Parameters were obtained from Fig. 7 according to Eq. (12).
[b] Predictions were based on Monte Carlo calculations of transmission,[32] using optical parameters $\mu$ and $L$ obtained by fitting Eq. (12) to the data shown in Fig. 7.
[c] Values were obtained from Ref. 34.
[d] Values were predicted[33] by Kubelka–Munk theory applied to measurements of the transmission of diffuse light through thin dermal sections.

Also, for very small values of $\rho$ the actual behavior of photons in tissue may differ from that predicted by this model. We are currently refining the model in order to consider these aspects of the problem, and we are assessing the significance of anisotropic scattering centers. Attention also is being given to the effects of possible macroscopic spatial inhomogeneities in the optical parameters.

## ACKNOWLEDGMENT

S. Havlin gratefully acknowledges financial support from the USA–Israel Binational Science Foundation.

## REFERENCES

1. R. L. Longini and R. Zdrojkowski, "A note on the theory of backscattering of light by living tissue," IEEE Trans. Biomed. Eng. **BME-15,** 4–10 (1968).
2. L. Reynolds, C. Johnson, and A. Ishimaru, "Diffuse reflectance from a finite blood medium: applications to the modeling of fiber optic catheters," Appl. Opt. **15,** 2059–2067 (1976).
3. R. A. J. Groenhuis, H. A. Ferweda, and J. J. Ten Bosch, "Scattering and absorption of turbid materials determined from reflection measurements. 1: Theory." Appl. Opt. **22,** 2456–2462 (1983).
4. R. A. J. Groenhuis, J. J. Ten Bosch, and H. A. Ferwerda, "Scattering and absorption of turbid materials determined from reflection measurements. 2: Measuring method and calibration," Appl. Opt. **22,** 2463–2467 (1983).
5. C. C. Johnson, "Optical diffusion in blood," IEEE Trans. Biomed. Eng. **BME-17,** 129–133 (1970).
6. R. J. Zdrojkowski and N. R. Pisharoty, "Optical transmission and reflection by blood," IEEE Trans. Biomed. Eng. **BME-17,** 122–128 (1970).
7. A. J. Tahmoush, P. D. Bowen, R. F. Bonner, T. J. Mancini, and W. K. Engel, "Laser Doppler blood flow studies during open-muscle biopsy in patients with neuromuscular diseases," Neurology **33,** 547–551 (1983).
8. G. P. Rodgers, A. N. Schechter, C. T. Noguchi, H. G. Klein, A. W. Nienhuis, and R. F. Bonner, "Periodic microcirculatory flow in patients with sickle-cell disease," New Engl. J. Med. **311,** 1534–1538 (1984).
9. H. M. Druce, R. F. Bonner, P. Choo, C. Patow, R. Summers, and M. A. Kaliner, "Response of nasal blood flow to neurohormones as measured by laser-Doppler velocimetry," J. Appl. Physiol. **57,** 1276–1283 (1984).
10. W. F. Larrabee, G. D. Sutton, A. Holloway, and G. Tolentino, "Laser Doppler-velocimetry and fluorescein dye in the prediction of skin flap viability, a comparison," Arch. Otolaryngol. **109,** 454–456 (1983).
11. R. F. Bonner, T. R. Clem, P. D. Bowen, and R. L. Bowman, "Laser-Doppler real-time monitor of pulsatile and mean blood flow in tissue microcirculation," in *Scattering Techniques Applied to Supramolecular and Nonequilibrium Systems,* S. H. Chen, B. Chu, and R. Nossal, eds, Volume 3 of NATO ASI Series B (Plenum, New York, 1981), pp. 685–701.
12. R. Bonner and R. Nossal, "Model for laser Doppler measurements of blood flow in tissue," Appl. Opt. **20,** 2097–2107 (1981).
13. M. D. Stern, "Laser-Doppler velocimetry in blood and multiple scattering fluids: theory," Appl. Opt. **24,** 1968–1986 (1985).
14. D. W. Lubbers, "Spectroscopic examination of tissue oxygenation," in *Oxygen Tranport to Tissue,* H. I. Bicher and D. Bruley, eds. (Plenum, New York, 1973), pp. 45–54.
15. R. N. Pittman and B. R. Duling, "Measurement of percent oxyhemoglobin in the microvasculature," J. Appl. Physiol. **38,** 321–327 (1975).
16. P. W. Cheung, S. Takatani, and E. A. Ernst, "Multiple wavelength reflectance oximetry in peripheral tissues," in *Oxygen Transport to Tissue,* I. A. Silver, M. Erecinska, and H. I. Bicher, eds. (Plenum, New York, 1978), pp. 69–75.
17. A. Mayevsky and B. Chance, "Intracellular oxidation-reduction state measured *in situ* by a multichannel fiber-optic surface fluorometer," Science **217,** 537–540 (1982).
18. B. Chance, N. Oshino, T. Sugano, and A. Mayevsky, "Basic principles of tissue oxygen determination from mitochondrial signals," Adv. Exp. Med. Biol. **37,** 277–292 (1973).
19. T. J. Dougherty, J. E. Kaufman, A. Goldfarb, K. R. Weishaupt, D. G. Boyle, and A. Mittelman, "Photoradiation therapy for the treatment of malignant tumors," Cancer Res. **38,** 2628–2635 (1978).
20. D. R. Dorion, L. O. Svaasand, and A. E. Profio, "Light dosimetry in tissue, application to photoradiation therapy," in *Porphyrin Photosensitization,* D. Kessel and T. J. Dougherty, eds. (Plenum, New York, 1983), pp. 63–76.
21. H. C. van de Hulst, *Multiple Light Scattering* (Academic, New York, 1980), Vol. 2.
22. P. Kubelka, "New contributions to the optics of intensely light-scattering materials. Part I," J. Opt. Soc. Am. **38,** 448–457 (1948); "New contributions to the optics of intensely light-scattering materials. Part II: nonhomogeneous layers," J. Opt. Soc. Am. **44,** 330–335 (1954).
23. J. T. Atkins, "Optical properties of turbid materials," in *The Biological Effects of Ultraviolet Radiation,* F. Urbach, ed. (Pergamon, Oxford, 1968), pp. 141–149.
24. V. Twersky, "Interface effects in multiple scattering by large, low-refracting, absorbing particles," J. Opt. Soc. Am. **60,** 908–914 (1970).
25. V. Twersky, "Absorption and multiple scattering by biological suspensions," J. Opt. Soc. Am. **60,** 1084–1089 (1970).
26. A. Ishimaru, "Theory and application of wave propagation and scattering in random media," Proc. IEEE **65,** 1030–1061 (1977).
27. G. D. Pedersen, N. J. McCormick, and L. O. Reynolds, "Transport calculations for light scattering in blood," Biophys. J. **16,** 199–207 (1976).
28. K. M. Case and P. F. Zweifel, *Linear Transport Theory* (Addison-Wesley, Reading, Mass., 1967).
29. A. Ishimaru, *Wave Propagation and Scattering in Random Media* (Academic, New York, 1978), Vol. 1.
30. J. J. Duderstadt and W. R. Martin, *Transport Theory* (Wiley-Interscience, New York, 1979).
31. G. H. Weiss and R. J. Rubin, "Random walks, theory and selected applications," Adv. Chem. Phys. **52,** 363–505 (1983).
32. R. R. Anderson and J. A. Parrish, "The optics of human skin," J. Invest. Dermatol. **77,** 13–19 (1981).
33. P. J. Kolari, "Penetration of unfocused laser light into the skin," Arch. Dermatol. Res. **277,** 342–344 (1985).